

How the Liquid-Liquid Transition Affects Hydrophobic Hydration in Deeply Supercooled Water

Dieter M. Paschek

Physikalische Chemie, Universitat Dortmund, Otto-Hahn-Str. 6, D-44221 Dortmund, Germany
(Dated: January 26, 2020)

We determine the phase diagram of liquid supercooled water by extensive computer simulations using the TIP5P-E model [J. Chem. Phys. 120, 6085 (2004)]. We find that the transformation of water into a low density liquid in the supercooled range strongly enhances the solubility of hydrophobic particles. The transformation of water into a tetrahedrally structured liquid is accompanied by a minimum in the hydration entropy and enthalpy. The corresponding change in sign of the solvation heat capacity indicates a loss of one characteristic signature of hydrophobic hydration. The observed behavior is found to be qualitatively in accordance with the predictions of the information theory model of Garde et al. [Phys. Rev. Lett. 77, 4966 (1996)].

The thermodynamical anomalies of liquid water are considered to be caused by a transformation between two different liquid forms of water buried in the deeply supercooled region [1]. The two different dense liquids have well characterized counterparts in the glassy state: The (very) high density and low density amorphous ice forms [2, 3]. Computer simulation studies have furnished a picture of a first order liquid-liquid phase transition between two liquids ending up in a metastable critical point [4, 5]. Although singularity free scenarios might as well explain the properties of supercooled water [1], there is experimental support for the liquid-liquid critical point hypothesis from the changing slope of the metastable melting curves observed for different ice polymorphs [6, 7]. To make the situation even more puzzling, recent computer simulations provide evidence that there might be even more than one liquid-liquid transition [8].

One prominent anomaly of liquid water is the increasing solubility of hydrophobic gases with decreasing temperature [9]. This behavior is the consequence of a negative solvation entropy of small hydrophobic particles [10]. Since the corresponding solvation enthalpy is also negative, the observed low solubility (the large positive solvation free energy) of small hydrophobic particles is basically due to a strong entropy effect. The origin of the negative hydration entropy is widely regarded as being due to the bias in the hydration waters orientational space, as the water molecules are trying to preserve their hydrogen bond network [11]. Entropy and enthalpy effects have been shown to be determined by the water in the first hydration shell [12]. In addition, the broken hydrogen bond states, with hydrogen bond donors/acceptors pointing towards the hydrophobic particles, are increasingly populated with increasing temperature [11]. Hence, the positive solvation heat capacity of hydrophobic particles is considered as one of the key signatures for hydrophobic hydration [13]. A recent experimental study of Souda [14], investigating alkane layers adsorbed on an amorphous solid water substrate, shows that the alkane phase gets soaked into the water phase in the temperature region close to the suspected glass transition tem-

perature [15]. One possible explanation (among others) might be that the highly viscous low density liquid form of water provides a significantly increased solubility for hydrophobic molecules. The scope of the present contribution is to monitor hydration of a small hydrophobic particle as we penetrate the deeply supercooled region. Our particular interest is to elucidate how the transformation into a low density, highly tetrahedrally ordered liquid phase [16] affects hydrophobic hydration.

The technical key problem regarding simulations of highly viscous liquids close to the glass transition is, of course, to provide proper sampling. To overcome this problem we perform parallel tempering simulations of an extended ensemble of states [17]. Here we use the technique of volume-temperature replica exchange molecular dynamics simulation (VTREM), which has been recently introduced by us to study the reversible pressure/temperature induced unfolding of small proteins [18]. To represent liquid supercooled water we employ the recently proposed TIP5P-E model for water, which was fitted to reproduce waters density maximum and related thermodynamical anomalies as closely as possible while treating the Coulomb interactions with the Ewald sum [19]. For the VTREM simulation [20] we consider a grid of 440 (V,T)-states. The state-points are represented by the temperatures 170.0 K, 181.6 K, 192.8 K, 203.5 K, 213.5 K, 222.7 K, 230.8 K, 238.0 K, 244.8 K, 251.8 K, 259.1 K, 266.9 K, 275.2 K, 284.2 K, 293.8 K, 304.3 K, 315.5 K, 327.8 K, 341.3 K and 356.3 K at the densities 0.890 g cm⁻³, 0.905 g cm⁻³, 0.920 g cm⁻³, 0.935 g cm⁻³, 0.950 g cm⁻³, 0.965 g cm⁻³, 0.980 g cm⁻³, 0.995 g cm⁻³, 1.010 g cm⁻³, 1.025 g cm⁻³, 1.040 g cm⁻³, 1.055 g cm⁻³, 1.070 g cm⁻³, 1.085 g cm⁻³, 1.100 g cm⁻³, 1.115 g cm⁻³, 1.130 g cm⁻³, 1.145 g cm⁻³, 1.160 g cm⁻³, 1.175 g cm⁻³, 1.190 g cm⁻³ and 1.205 g cm⁻³. Starting from a set of equilibrated initial configurations obtained at ambient conditions, the VTREM simulation [21] was conducted for 20 ns, providing a total 8.8 s worth of trajectory data. The average time interval between two successful exchanges was obtained to be about 3 ps. During the entire course of the simulation each replica has crossed

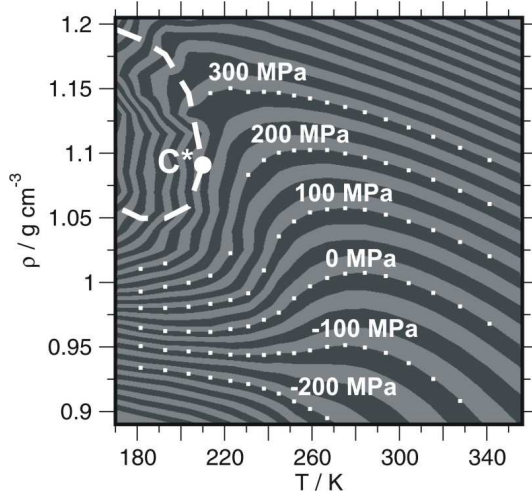


FIG. 1: Phase diagram for stable and supercooled liquid TIP5P-E water according to the V TREMDP(ρ ; T) data set. The spacing between different contour colours is according to a pressure drop of 25 MPa. Selected isobars are indicated. The high density / low density liquid (LDL/LDL) coexistence line is given by the heavy dashed line. The corresponding LDL/LDL critical point is denoted by C with $T = 210$ K, $P = 310$ MPa and $\rho = 1.09$ g cm $^{-3}$.

the whole temperature and density interval several times. Quickly, after an initial equilibration period of about 4 ns, the average pressure and potential energies show convergence even for the lowest temperatures and the remaining 16 ns are used for analysis.

Figure 1 shows the phase diagram of liquid supercooled water in terms of a contour plot of the $P(\rho; T)$ -data as obtained by the V TREMD simulations. The TIP5P-E phase diagram apparently exhibits a first order phase transition between two metastable liquid phases, ending in a second critical point C. The location of the coexistence line, estimated from a Maxwell construction using the subcritical isotherms, has to be seen as a rough guess only, since the exact form of the van der Waals loops in the two phase region might depend on the system size. The location of C is close to the values reported by Yamada et al. for the original TIP5P model with $T = 217$ K, $P = 340$ MPa and $\rho = 1.13$ g cm $^{-3}$ [23]. Figure 2a compares several selected isobars according to linear interpolation from the TIP5P-E $P(\rho; T)$ data set with the experimental data after Wagner and Pinn [22]. Although the location of the density maximum at normal pressure is close to the experimental values, the TIP5P-E model indicates a considerably larger thermal expansivity as the real water and is significantly less compressible. Figure 2b shows that the isobars derived from V TREMD data set match exactly with data obtained from conventional NPT-simulations. For comparison the isobar according to Ricks simulations is shown [19]. We denote small, but significant differences. Since both simulations were using Ewald summation, we can just speculate about their ori-

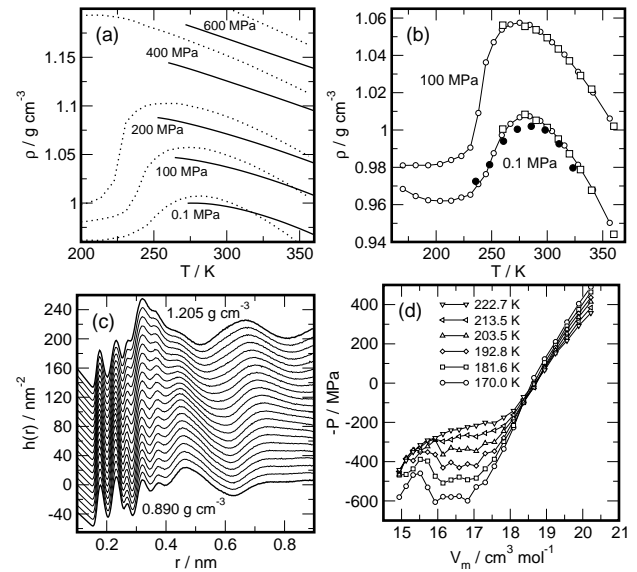


FIG. 2: (a): Selected isobars for TIP5P-E water (dotted lines) compared with experimental data of Ref. [22]. (b) Two isobars for TIP5P-E. Open circles: Data obtained by linear interpolation from the V TREMDP(ρ ; T) data set. Open squares: Data obtained by conventional constant temperature/constant pressure MD simulations. Filled circles: Data according to S.W.Ricks [19]. (c) $h(r) = 4 \sum_{N=V} (0.092 g_{OO}(r) + 0.486 g_{HH}(r) + 0.422 g_{OH}(r)) - 1$ – functions for the 222.7 K isotherm. The functions are shifted by an increment of 10 nm $^{-2}$. (d) Near- and sub-critical isotherms.

gin. An explanation might be a possible absence of long range Lennard-Jones pressure corrections in Ref. [19]. We would like to emphasize one particular detail of the low pressure isobars as indicated in Figures 1 and 2b: The density goes through a minimum after the transformation into the low density liquid has taken place. Apparently at low temperatures the expansivity seems to behave as it would be expected for a conventional liquid. I.Brovchenko [8] and recently P.H.Poole [24] have made similar observations for the ST2 model. Figure 2c shows the evolution of the composite radial distribution function $h(r)$ along the 222.7 K-isotherm. The highlighted patterns obtained for the lowest and highest densities show strong similarity with the functions determined experimentally by Bellissent-Funel et al. for high and low density amorphous ice [25]. The observed low density pattern has been shown to be connected with a highly tetrahedral order in the first hydration shell around each water molecule [16]. Similarities between the local structure of LDA and ice Ih have also been demonstrated recently by Finney et al. from the analysis of neutron scattering experiments [26]. We do not observe indications for the presence of further liquid-liquid transitions for TIP5P-E, as suggested by Brovchenko et al. for the ST2 model [8]. However, further phase transitions might be present at even lower temperatures. Finally, no signs

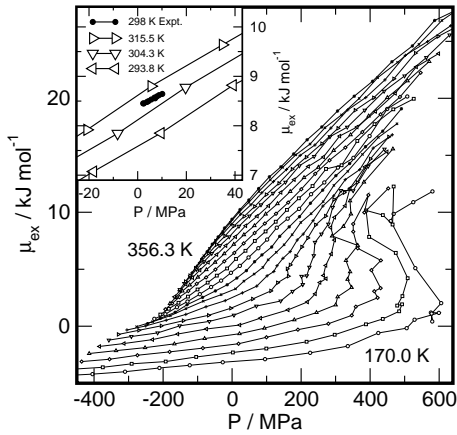


FIG. 3: Excess chemical potential for Ar dissolved in TIP5P-E water as a function of pressure and temperature. The lines indicate all calculated isotherms ranging from 170 K to 356.3 K. The inset shows the experimental data of Kennan and Pollack [27] with the simulation data. Although the experimental pressure interval is much smaller compared to the pressure range of our study, the coincidence is quite remarkable. The most prominent feature, the decreasing solubility with increasing pressure, is found to be well reproduced. The pressure dependence is expressed by a partial molar volume of $30 \text{ cm}^3 \text{ mol}^{-1}$, quite close to the experimental value of $25 \text{ cm}^3 \text{ mol}^{-1}$ [31]. Two regimes of small and strong pressure dependence are denoted, obviously related to the transformation between the high and low density liquid forms of water. We would like to emphasize that we find an increase of the partial molar volume for Ar around normal pressure for the 260–255 K isotherms. Kennan and Pollack made a similar observation for Xenon around 298 K. If, and how these two observations are related has to be further investigated.

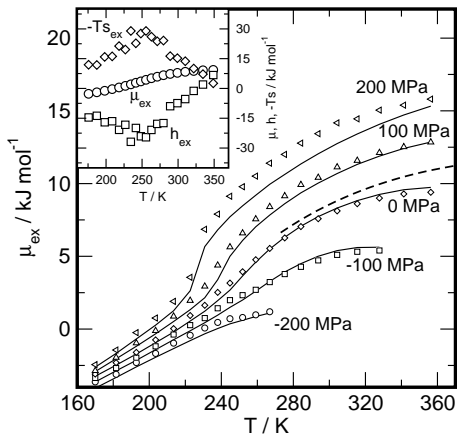


FIG. 4: The symbols indicate representative isobars obtained from the $\mu_{\text{ex}}(P; T)$ TIP5P-E data set. The dashed line indicates the experimental data for 0.1 MPa [28]. The full lines represent predictions for $\mu_{\text{ex}} = aT^2 + b$ according to the leading term in the information theory model [29] with $a = 8 \times 10^2 \text{ kJ mol}^{-1} \text{ K}^{-1} \text{ cm}^3 \text{ g}^{-1}$ and $b = -16 \text{ kJ mol}^{-1}$. The inset shows the enthalpy (h_{ex}) and entropy ($T s_{\text{ex}}$) contributions to the excess chemical potential for the simulated 0 MPa isobar.

for crystallization are observed, as denoted by Yamada et al. [23]. Probably our smaller system size and the random walk of the replicas through state-space, regularly reaching stable regions, prevents the systems from crystallizing.

The hydrophobic hydration of a Lennard-Jones Ar atom ($A_{\text{Ar}} = 0.3290 \text{ nm}$ and $A_{\text{Ar}} = k = 98.9 \text{ K}$) [30] is given as excess chemical potential $\mu_{\text{ex}} = -\frac{1}{2} \ln \left(1 - \frac{1}{2} \frac{h_{\text{ex}}}{kT} \right)$ for infinite dilution, where h_{ex} is the solubility and $k = 1 = kT$. We employ the Widom particle insertion method [17] with $\mu_{\text{ex}} = -\frac{1}{2} \ln \left(\frac{h_{\text{ex}}(P)}{h_{\text{ex}}(0)} \right)$, where $h_{\text{ex}}(P)$ is the energy of an inserted test-particle. The brackets $h_{\text{ex}}(P)$ indicate

canonical sampling. Details about the calculation are given elsewhere [30]. Figure 3 shows the excess chemical potential for Ar dissolved in TIP5P-E water for all simulated state points. First of all we would like to emphasize that the solubility increases strongly when penetrating the deeply supercooled region with μ_{ex} becoming even negative. The inset of Figure 3 compares the experimental data of Kennan and Pollack [27] with the simulation data. Although the experimental pressure interval is much smaller compared to the pressure range of our study, the coincidence is quite remarkable. The most prominent feature, the decreasing solubility with increasing pressure, is found to be well reproduced. The pressure dependence is expressed by a partial molar volume of $30 \text{ cm}^3 \text{ mol}^{-1}$, quite close to the experimental value of $25 \text{ cm}^3 \text{ mol}^{-1}$ [31]. Two regimes of small and strong pressure dependence are denoted, obviously related to the transformation between the high and low density liquid forms of water. We would like to emphasize that we find an increase of the partial molar volume for Ar around normal pressure for the 260–255 K isotherms. Kennan and Pollack made a similar observation for Xenon around 298 K. If, and how these two observations are related has to be further investigated. Figure 4 shows the temperature dependence of μ_{ex} for several selected isobars ranging from 200 MPa to 200 MPa. The 0.1 MPa isobar according to Fernandez-Priani and Crochet [28] is given for comparison. From computer simulations of water, S. Garde et al. have derived an information theory (IT) model [29, 32], giving simple analytic expressions for the hydrophobic hydration as a function of temperature and density. The leading term in the IT model strongly suggests a quadratic relation between the excess chemical potential and the water number density according to $\mu_{\text{ex}} = k \frac{2}{3} T v^2 = \frac{2}{3} \frac{n^2}{v} \ln \left(\frac{v}{n} \right)$ [32], where v denotes the volume of the size of a hydrophobic hard sphere particle, while $\frac{2}{3} = \frac{n^2}{v} \ln \left(\frac{v}{n} \right)$ indicates the variance of the number of water molecules in a sphere of volume v . The lines in Figure 4 indicate a temperature dependence as suggested by the information theory model, assuming the term $v^2 = \frac{2}{3} \frac{n^2}{v}$ as being constant (and the same for all isobars shown here) and shifting the isobars by a constant offset to account for attractive interactions. The relation describes the behavior for the supercooled state almost quantitatively for a broad pressure range. Particularly well reproduced is the change in slope when passing the transformation into the low density liquid. As shown in the inset of Figure 4, the change in slope of μ_{ex} is related to the minimum in the entropy and enthalpy contributions. The minimum in the enthalpy causes a change in sign of the corresponding heat capacity contribution from positive at high temperatures to negative for the low density liquid. Apparently, a prominent signature of the "hydrophobic hydration" vanishes while passing the transition at about 250 K. In line with the interpretation of hydrophobic effects as de-

rived from of the simplified MB model for water at ambient conditions [11], the scenario is explained as follows: In the low-temperature/low-density regime, waters coordination number approaches four, while the structure is that of a very homogeneous tetrahedral network. Due to the lack of further possible hydrogen binding partners, the situation for water molecules in the bulk and in the hydrophobic hydration shell is therefore less diverse than it is for water molecules in the "high density liquid" observed at ambient temperatures. Consequently, a larger hydrophobic particle might even introduce further disorder into the stretched hydrogen bond network and might thus even experience a positive hydration entropy in the supercooled low density state. Therefore, a further investigation on particle size dependence, hydrophobic aggregates and hydrophobic interaction might reveal a behavior completely different from that supposed for ambient conditions [33]. More new insights in the phenomena of the hydrophobic effects might be expected.

This work was supported by DFG FOR 436. I would like to thank Angel E. Garcia, Ivan Brovchenko and Alfonso Geiger for valuable discussions.

ulation. From Algorithms to Applications (Academic Press, San Diego, 2002), 2nd ed.

- [18] D. Paschek and A. E. Garcia, *Phys. Rev. Lett.* **93**, 238105 (2004).
- [19] S. W. Rick, *J. Chem. Phys.* **120**, 6085 (2004).
- [20] State swapping moves between two states i and j are accepted with a probability $P_{\text{acc}} = \min\{1, \exp[-\beta(U(s_i^N; L_i) - U(s_j^N; L_i) + U(s_j^N; L_j) - U(s_i^N; L_j))]\}$. Here, s_N^N represents the set of scaled coordinates $s_N = L^{-1} r_N$ of the entire N -particle system belonging to state i . $U(s_i^N; L_i)$ denotes the potential energy of conformation s_i^N at volume $V_i = L_i^3$, whereas $U(s_i^N; L_j)$ represents the conformational energy belonging to s_i^N at volume V_j . The decision whether a state swapping move or an MD move is executed, is chosen at random with a probability of 0.2 to select a state swapping move.
- [21] Each replica represents a molecular dynamics (MD) simulation of 256 molecules in the NVT ensemble. The electrostatic interactions are treated by the Ewald summation [34] with a real space cutoff of 0.9 nm and a 18 × 18 × 18 mesh with 4th order interpolation for the reciprocal lattice contribution. Lennard-Jones cutoff corrections for energy and pressure have been taken into account. A 2 fs timestep was used. The simulations were carried out using the GROMACS 3.2 program [35], modified by us in order to allow for V-T-state-swapping moves. The temperature tiling has been chosen to maintain an acceptance ratio of about 0.2 for state swapping.
- [22] W. Wagner and A. P. Russell, *J. Phys. Chem. Ref. Data* **31**, 387 (2002).
- [23] M. Yamada, S. Mossa, H. E. Stanley, and F. Sciortino, *Phys. Rev. Lett.* **88**, 195701 (2002).
- [24] P. H. Poole, private communication.
- [25] M. C. Bellissent-Funel, J. Teixeira, and L. Bosio, *J. Chem. Phys.* **87**, 2231 (1987).
- [26] J. L. Finney, A. Hallbrucker, I. Kohl, A. K. Soper, and D. T. Bowron, *Phys. Rev. Lett.* **88**, 225503 (2002).
- [27] R. P. Kennan and G. L. Pollack, *J. Chem. Phys.* **93**, 2724 (1990).
- [28] R. Fernandez-Prini and R. C. Roettger, *J. Phys. Chem. Ref. Data* **18**, 1231 (1989).
- [29] S. Garde, G. Hummer, A. E. Garcia, M. E. Paulaitis, and L. R. Pratt, *Phys. Rev. Lett.* **77**, 4966 (1996).
- [30] D. Paschek, *J. Chem. Phys.* **120**, 6674 (2004).
- [31] When fitting the ex-data for Argon of Ref. [27].
- [32] G. Hummer, S. Garde, A. E. Garcia, and L. R. Pratt, *Chem. Phys.* **258**, 349 (2000).
- [33] D. Huang and D. Chandler, *Proc. Natl. Acad. Sci. USA* **97**, 8324 (2000).
- [34] U. Essmann, L. Perera, M. L. Berkowitz, T. A. Darden, H. Lee, and L. G. Pedersen, *J. Chem. Phys.* **103**, 8577 (1995).
- [35] E. Lindahl, B. Hess, and D. van der Spoel, *J. Mol. Model.* **7**, 306 (2001).

[1] P. G. Debenedetti, *J. Phys. Cond. Matt.* **15**, R1669 (2003).

[2] O. Mishima, L. D. Calvert, and E. W. Halley, *Nature* **310**, 393 (1984).

[3] T. Loerting, C. Salzmann, I. Kohl, E. Mayr, and A. Hallbrucker, *Phys. Chem. Chem. Phys.* **3**, 5355 (2001).

[4] P. H. Poole, F. Sciortino, U. Essmann, and H. E. Stanley, *Nature* **360**, 324 (1992).

[5] H. Tanaka, *Nature* **380**, 328 (1996).

[6] O. Mishima and H. E. Stanley, *Nature* **396**, 329 (1998).

[7] O. Mishima, *Phys. Rev. Lett.* **85**, 334 (2000).

[8] I. Brovchenko, A. Geiger, and A. O. Leznikova, *J. Chem. Phys.* **118**, 9473 (2003).

[9] E. W. Ilhamed, R. Battino, and R. J. Wilcox, *Chem. Rev.* **77**, 219 (1977).

[10] L. R. Pratt, *Annu. Rev. Phys. Chem.* **53**, 409 (2003).

[11] N. T. Southall, K. A. Dill, and A. D. J. Haymet, *J. Phys. Chem. B* **106**, 521 (2002).

[12] D. Paschek, *J. Chem. Phys.* **120**, 10605 (2004).

[13] K. A. T. Silverstein, A. D. J. Haymet, and K. A. Dill, *J. Am. Chem. Soc.* **122**, 8037 (2000).

[14] R. Souda, *J. Chem. Phys.* **121**, 8676 (2004).

[15] O. Mishima, *J. Chem. Phys.* **121**, 3161 (2004).

[16] D. Paschek and A. Geiger, *J. Phys. Chem. B* **103**, 4139 (1999).

[17] D. Frenkel and B. Smit, *Understanding Molecular Simulation*